Author's Accepted Manuscript

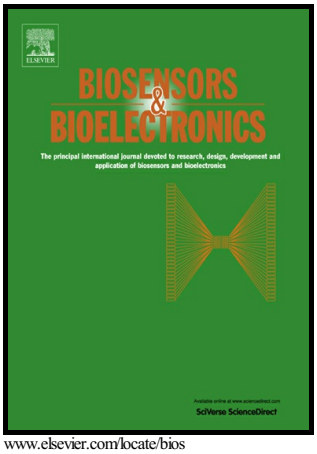

www.elsevier.com/locate/bios

A novel DNA biosensor integrated with Polypyrrole/streptavidin and au-PAMAM-CP bionanocomposite probes to detect the rs4839469 locus of the *vangl1* gene for dysontogenesis prediction

Qingying Li, Chao Yu, Rufei Gao, Chunyong Xia, Guolin Yuan, Yuliang Li, Yilin Zhao, Qiutong Chen, Junlin He

PII: S0956-5663(16)30132-4
DOI: http://dx.doi.org/10.1016/j.bios.2016.02.025
Reference: BIOS8457

To appear in: *Biosensors and Bioelectronic*

Received date: 15 December 2015
Revised date: 31 January 2016
Accepted date: 9 February 2016

Cite this article as: Qingying Li, Chao Yu, Rufei Gao, Chunyong Xia, Guolin Yuan, Yuliang Li, Yilin Zhao, Qiutong Chen and Junlin He, A novel DNA biosensor integrated with Polypyrrole/streptavidin and au-PAMAM-CP bionanocomposite probes to detect the rs4839469 locus of the *vangl1* gene for dysontogenesis prediction, *Biosensors and Bioelectronic* http://dx.doi.org/10.1016/j.bios.2016.02.025

This is a PDF file of an unedited manuscript that has been accepted for publication. As a service to our customers we are providing this early version of the manuscript. The manuscript will undergo copyediting, typesetting, and review of the resulting galley proof before it is published in its final citable form. Please note that during the production process errors may be discovered which could affect the content, and all legal disclaimers that apply to the journal pertain.

ACCEPTED MANUSCRIPT

A novel DNA biosensor integrated with polypyrrole/streptavidin and Au-PAMAM-CP bionanocomposite probes to detect the rs4839469 locus of the *vangl1* gene for dysontogenesis prediction

Qingying Li[1], *Chao Yu*[1], *Rufei Gao, Chunyong Xia, Guolin Yuan, Yuliang Li, Yilin Zhao, Qiutong Chen, Junlin He* *

School of Public Health and Management, Institute of Life Science, Chongqing Medical University, Chongqing 400016, P. R. China

[1]Chao Yu and *Qingying Li* contributed equally to this work.

*Corresponding author: Prof. Junlin He,

Email: hejunlin_11@aliyun.com

Tel: (86) 23-68485926

Fax: (86) 23-68485008

Full address: Box 197, Chongqing Medical University, No.1 Yixueyuan Road, Yuzhong District, Chongqing 400016, P. R. China.

Accepted manuscript

ACCEPTED MANUSCRIPT

ABSTRACT

The single nucleotide polymorphism (SNP) of the *vangl1* gene is highly correlated with Neural Tube Defects (NTDs), a group of severe congenital malformations. It is hindered by the lack of a quantitative detection method. We first propose the use of a DNA biosensor to detect the missense single nucleotide polymorphism (rs4839469 c.346G > A p.Ala116Thr) of the *vangl1* gene in this work. Polypyrrole (PPy) and streptavidin were integrated to modify a gold electrode. We took advantage of the PPy's good biocompatibility and excellent conductivity. To further accelerate the electron transfer process at the electrode surface, polyamidoamine dendrimer-encapsulated gold nanoparticles (Au-PAMAM) were used, because Au-PAMAM possess a large number of amino groups to load capture probes (CP). Using the biotin-streptavidin system, the Au-PAMAM-CP bionanocomposite probe, which can detect the target DNA, was conjugated to the electrode surface. Under optimal conditions, the DNA biosensor exhibited a wide linear range of 0.1 nM to 100 nM with a low detection limit of 0.033 nM (S/N = 3). The results suggest that this approach has the potential to be used in clinical research.

Keywords: PPy/ streptavidin; Au-PAMAM; capture probe; DNA biosensor

Accepted manuscript

ACCEPTED MANUSCRIPT

1. Introduction

Both genetic and nongenetic factors are involved in the aetiology of dysontogenesis, such as Neural Tube Defects (NTDs), which are a group of birth anomalies resulting from the failure of fusion of the neural tube around the 28th day after conception. Maternal folate deficiency plays an important role in the occurrence of NTDs. The missense single nucleotide polymorphism (SNP) (rs4839469 c.346G > A p.Ala116Thr) in the coding region of the *vangl1* gene is also highly associated with the occurrence of NTDs. The genotype GC in the rs4839469 allele of *vangl1* increased the risk of NTDs (Cai et al. 2014). Thus, SNPs of the *vangl1* gene could be used as a new valuable biomarker for clinical diagnosis (Chang et al. 2015). With this consideration, the determination of a specific DNA segment determination of the *vangl1* gene is of great importance for an early diagnosis.

Various techniques for SNP genotyping have been reported, such as DNA sequencing (Bradbury et al. 2015; Syvänen 2001), mass spectroscopy (Meyer et al. 2015; Stepanov and Trifonova 2013), real-time quantitative reverse transcription polymerase chain reaction (RT-PCR) (Fujii et al. 2000; Maekawa et al. 2015), and DNA microarray (Russom et al. 2006; Wang et al. 2014) and so on. However, all types of drawbacks largely limit the application of these methods in the clinical setting. DNA sequencing relies on the interpretation of an indirectly measured signal (e.g., current, position, speed, force, etc.) into a molecular property and wastes a great deal of operation time (Liang et al. 2015); Mass spectroscopy**,** which is laborious and expensive, requires isotope labelling and lacks sensitivity and also relies on sophisticated instruments and skilled man power (Chen and Zhou 2015; Wang et al. 2016). RT-PCR is poorly suited for implementation due to the complicated sample pre-treatment, high-cost, relatively long detection time, need for trained technicians, and likelihood of false-negative results (Fu et al. 2016; Mohamed et al. 2004). DNA microarrays are expensive and require complex procedures; the reaction times for hybridization are also quite long to complete all of the hybridization reactions in a large-field area (Mogi et al. 2011). Compared with these methods, DNA biosensors

Accepted manuscript

ACCEPTED MANUSCRIPT

have received a large amount of attention because of their simplicity, rapidity and low cost (Ruiyi et al. 2015). Furthermore, DNA biosensors are highly sensitive and user-friendly and do not require sophisticated instruments (Yao et al. 2013). Thus, finding a highly sensitive and selective DNA-based electrochemical sensor for SNP genotyping appears to be a realistic goal (Liu et al. 2013; Shin et al. 2015). To the best of our knowledge, there is no report on the electrochemical detection of the *vangl1* gene yet. To develop an electrochemical biosensor for the detection of genotype GC in rs4839469 of the *vangl1* gene is both important and necessary.

Polypyrrole (PPy), a type of organic conducting polymer, has been widely used to modify electrodes to improve the sensitivity of electrochemical biosensors due to its interesting redox behaviour. PPy possesses good biocompatibility and can be immobilized for a variety of biomolecules different from conventional methods such as covalent binding (Cosnier 1999). Streptavidin-biotin binding has been widely used as a covalent bridge method in electrochemical biosensors (Jo et al. 2015; Li et al. 2015), because one streptavidin molecule can bind up to four biotin molecules and possesses the highest known affinity in nature (Livnah et al. 1993). In this study, using streptavidin as a dopant, a novel type of PPy/streptavidin film has been electrochemically co-deposited onto the surface of a gold electrode. It simplified the procedure and was proposed for the first time in DNA biosensors.

To further improve the sensitivity of the DNA biosensor, dual-amplification strategies based on the streptavidin-biotin system and bionanocomposite probe were proposed. Polyamidoamine (PAMAM) dendrimers are hyper-branched, tree-like molecules with a large number of amino groups to load capture probes (CP) and are able to effectively prevent nanoparticle aggregation (Cosnier 1999; Tomalia and Frechet 2002). However, PAMAM also decreased the conductivity of the modified materials, which limits its extensive application in the electrochemical biosensors (Kavosi et al. 2014). To overcome this limitation, previous experts shifted their attention to various nanoparticles, especially gold nanoparticles (AuNPs), which can help to strengthen the conductivity of PAMAM (Jeong et al. 2013; Kavosi et al. 2014; Zhang et al. 2013). Through amino-Au affinity, AuNPs can be steadily encapsulated

Accepted manuscript

ACCEPTED MANUSCRIPT

in PAMAM (Zhuo et al. 2010), which shows good dispersive stability and a smaller particle size compared with AuNPs prepared without a template (Zong et al. 2013). Therefore, polyamidoamine dendrimer-encapsulated gold nanoparticles (Au-PAMAM) were synthesized in this study to load a large quantity of CP to form the Au-PAMAM-CP bionanocomposite probe. Compared with single-stranded DNA, hairpin DNA probes have shown exceptional promise in electrochemical biosensors due to their conformational constraints (Kjällman et al. 2008), but have never been used to detect *vangl1* gene. The hairpin DNA probe, as a CP in this assay, possesses a carboxyl group at the 5' end and a biotin at the 3' end, leading to a considerable amount of CP labelling on Au-PAMAPM through an amide reaction, forming the Au-PAMAM-CP bionanocomposite probe. In the presence of DNA target, hybridization between the CP and target DNA causes a conformational change in the Au-PAMAM-CP. The biotin molecule that labelled the 5' end of Au-PAMAM-CP is then exposed to the electrode surface, which modified the PPy/streptavidin film. Through streptavidin-biotin binding, the electrode surface was covered with Au-PAMAM-CP; because of this redox moiety, the rate of electron transfer at the electrode surface was changed significantly.

This paper demonstrates a direct, sensitive and selective electrochemical DNA biosensing method using a novel stem-loop DNA biosensor modified by a PPy/streptavidin film. With the dual amplification strategy of the biotin-streptavidin system and a bionanocomposite probe, the sensitivity of the method was significantly increased. The stem-loop DNA biosensors developed in this study can be used to detect the *vangl1* gene in serum samples. To the best of our knowledge, this is the first report of the application of PPy/streptavidin in a DNA biosensor, and a new probe was created. At the same time, this study demonstrates the first electrochemical detection of specific DNA segment in the *vangl1* gene.

2. Experimental

2.1. Materials and reagents

Accepted manuscript

ACCEPTED MANUSCRIPT

The materials and reagents are described in detail in the Supplementary information (S11).

2.2. Apparatus

The apparatus are described in detail in the Supplementary information (S12).

2.3. Synthesis of the Au-PAMAM-CP bionanocomposite probe

First, Au-PAMAM was synthesized as previously described (Shen et al. 2015). Briefly, 2 mL of a $HAuCl_4$ solution (2 mM) was added to the solution containing 20 μL of PAMAM (0.5 g mL^{-1}) with stirring for 1 h, and 1 mL of $NaBH_4$ (20 mM) was quickly added to the solution with vigorously stirring. When Au-PAMAM formed, the solution colour immediately changed from light yellow to fuchsia. Thereafter, the reaction mixture was centrifuged at 12000 rpm for 30 min, and the pellet was resuspended in distilled water. Subsequently, a 10 μM solution of the CP, labelled at the 5'-COOH, was diluted with sodium phosphate buffer (0.1 M Na_2HPO_4/NaH_2PO_4, 0.1 M NaCl, 3.0 mM Mg^{2+}, pH 7.4) and slowly cooled to room temperature for at least 2 h after being heated at 95°C for 5 min. Next, 1 mL of freshly prepared PAMAM-Au nanocomposite, 500 μL of 100 mM EDC and 400 mM of a NHS solution were added and mixed gently for 4 h. The CP was conjugated onto the Au-PAMAM nanocomposite surfaces by the amide reaction. Excess reagents were removed by centrifuging at 12,000 rpm for 30 min. The Au-PAMAM-CP were suspended in a sodium phosphate buffer (0.1 M Na_2HPO_4/NaH_2PO_4, 0.1 M NaCl, 3.0 mM Mg^{2+}, pH 7.4) and preserved at 4℃.

2.4. Electropolymerization of the PPy/streptavidin film on gold electrodes

The PPy/streptavidin film was prepared through copolymerization of Py and

Accepted manuscript

ACCEPTED MANUSCRIPT

streptavidin with a constant potential technique as previously described (Xiao et al. 2007). Before the GE has been used, they were initially polished with 0.3 μm and 0.05 μm alumina slurries, and then washed successively with ethanol and water. Thereafter, it was electrochemically polished by scanning the potential from -0.2 to +1.6 V in 0.5 M H_2SO_4 at a scan rate of 0.1 V s^{-1} until a reproducible cyclic voltammogram was established to remove any remaining impurities, followed by rinsing with water and drying under a mild nitrogen stream. Then, electrochemical copolymerization was performed at 0.8 V for 4 min in a solution containing 0.1 M pyrrole, 0.02 M SDS, and 0.2 mg ml^{-1} streptavidin. The copolymerization solution was bubbled with nitrogen for 20 min before use every time. Finally, the modified electrode was incubated in a BSA solution (0.25%, w/v) for 1 h at room temperature to eliminate nonspecific binding sites between the analyte and the electrode.

2.5. Agarose gel electrophoresis for the characterization of CP

Agarose gel electrophoresis was performed to demonstrate the formation of the stem-loop structure of the CP. The analysis by electrophoresis was carried with 5% agarose gel electrophoresis run in 0.5×TBE buffer (pH 7.9) at room temperature, followed by nucleic acid dye staining. After loading 8 uL of each prepared sample into the lanes, the electrophoresis experiments were performed at a 90 V constant voltage for 1.5 h.

2.6. Detection of target DNA

The prepared Au-PAMAM-CP hybridized with different concentrations of target DNA in a sodium phosphate buffer (0.1 M Na_2HPO_4/NaH_2PO_4, 0.1 M NaCl, 3.0 mM Mg^{2+}, pH 7.4) at 35°C for 30 min. Then, the PPy/streptavidin modified electrode was immersed in the above mixture for 40 min to capture Au-PAMAM-CP-target DNA hybridization via the streptavidin-biotin binding method. This step was followed by washing the PPy/streptavidin film with 0.1% SDS (pH 7.4) to remove non-specific

Accepted manuscript

absorbents. The electrochemical measurements were carried out by DPV based on the increase in the current responses of Au-PAMAM, which were proportional to the concentrations of the target DNA. The DPV were performed in a 5 mM $[Fe(CN)_6]^{3+/4+}$ (0.1 M KCl) solution with a potential scan from -0.2 to 0.6 V. The target hybridization event was sensitively transduced by detecting the electrochemical reduction current signal of the Au-PAMAM-CP-target DNA, in the presence of target DNA; the immobilized CP was in the "closed" state. When hybridized with the target DNA, the CP was in the "open" state, forming a more stable, rigid target-probe duplex. Then the 3'-biotin could conjugate with the PPy/streptavidin through biotin-streptavidin binding. The CP had an advantage in mismatch discrimination as well. The fabrication procedure of the biosensor is illustrated in **Scheme 1.**

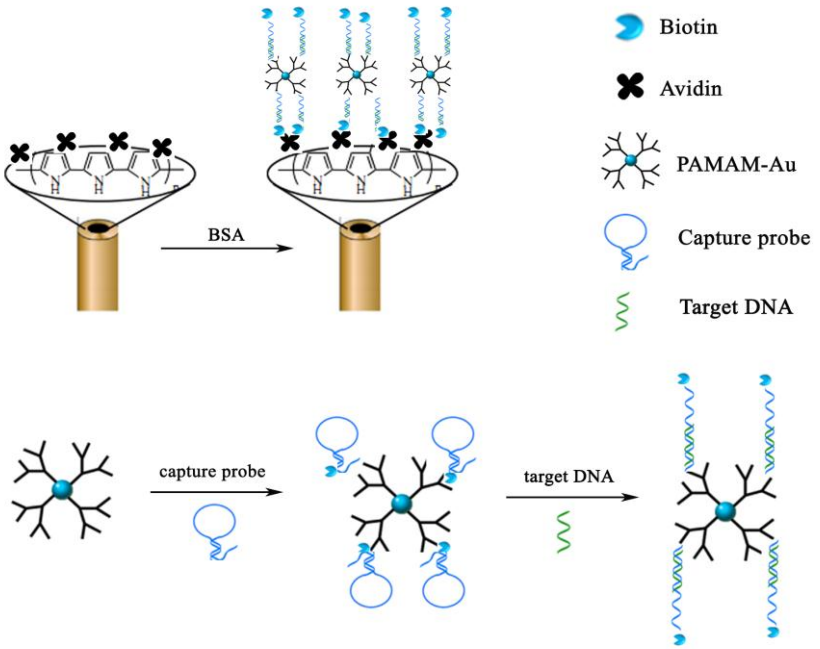

Sequences of Oligonucleotide Used in This Study

name	sequence (from 5' to 3')
Capture probe (CP)	HOOC-GCCTGC**TGGCAGCGG**
	AGAAAAGAAGCAGGC-biotin
Complementary DNA (Target DNA)	TTCTTTTCTCCGCTGCCA
Single-base mismatched DNA (SBM)	TTCTTTTCTCC**C**CTGCCA
Three-base mismatched DNA (TBM)	TTC**G**TTTCTCC**C**CTGC**T**A
Non-complementary DNA (ncDNA)	GCAGACAATGTCTCTATG

ACCEPTED MANUSCRIPT

Scheme 1. Schematic illustration of the electrochemical DNA assay

3. Results and discussion

3.1. Morphology and characterization of the PPy/streptavidin film

Three-dimensional laser scanning, SEM, FT-IR spectroscopy, and CV techniques were performed to characterize the PPy/streptavidin film. To confirm that PPy has been successfully deposited with streptavidin, Fig. 1A and B show a comparison of the morphology of the PPy film and PPy/streptavidin film scanned by a 3D laser scanning microscope. As shown in Fig. 1A, unmodified PPy film particles are uniform, with the highest peak height at 206.45 μm. Fig. 1B shows that the surface of PPy/streptavidin film was much flatter than the PPy film, with the highest peak height at 93.80 μm. The surface change was also demonstrated by SEM. As shown in Fig. 1C, the unmodified PPy film exhibited a globular and short rod-like submicron structure, with diameters ranging between 500 and 700 nm; this morphology was consistent with previous reports (Ghanbari and Hajheidari 2015). From Fig. 1D, it can be seen that the surface of the resultant PPy/streptavidin film was also much flatter than the PPy film due to the presence of protein molecules (Li et al. 2013), that blocked the grooves of the PPy surface, indicating that streptavidin was homogeneously embedded in the polymer film. A further demonstration of the formation of the PPy/streptavidin film is shown in Fig. 1E and F by FT-IR spectroscopy and CV technique. As shown in Fig. 1E, a comparison of the FT-IR spectrum of the PPy/streptavidin film with PPy showed that PPy/streptavidin (curve b) displays three protein characteristic peaks at 1432, 1548, and 1662 cm^{-1}, attributed to the successful embedding of streptavidin into the PPy film (Byler and Susi 1986). As shown in Fig. 1F, the CV result gave the conductivity of PPy and PPy/streptavidin film. Compared with PPy/streptavidin, the peak current of PPy was higher, the change of the current reached 318 μA (curve a), which was attributed to streptavidin hindering electron transfer as an insulating layer. FT-IR spectroscopy and the CV technique both illustrate that streptavidin was successfully incorporated onto the PPy

Accepted manuscript

film.

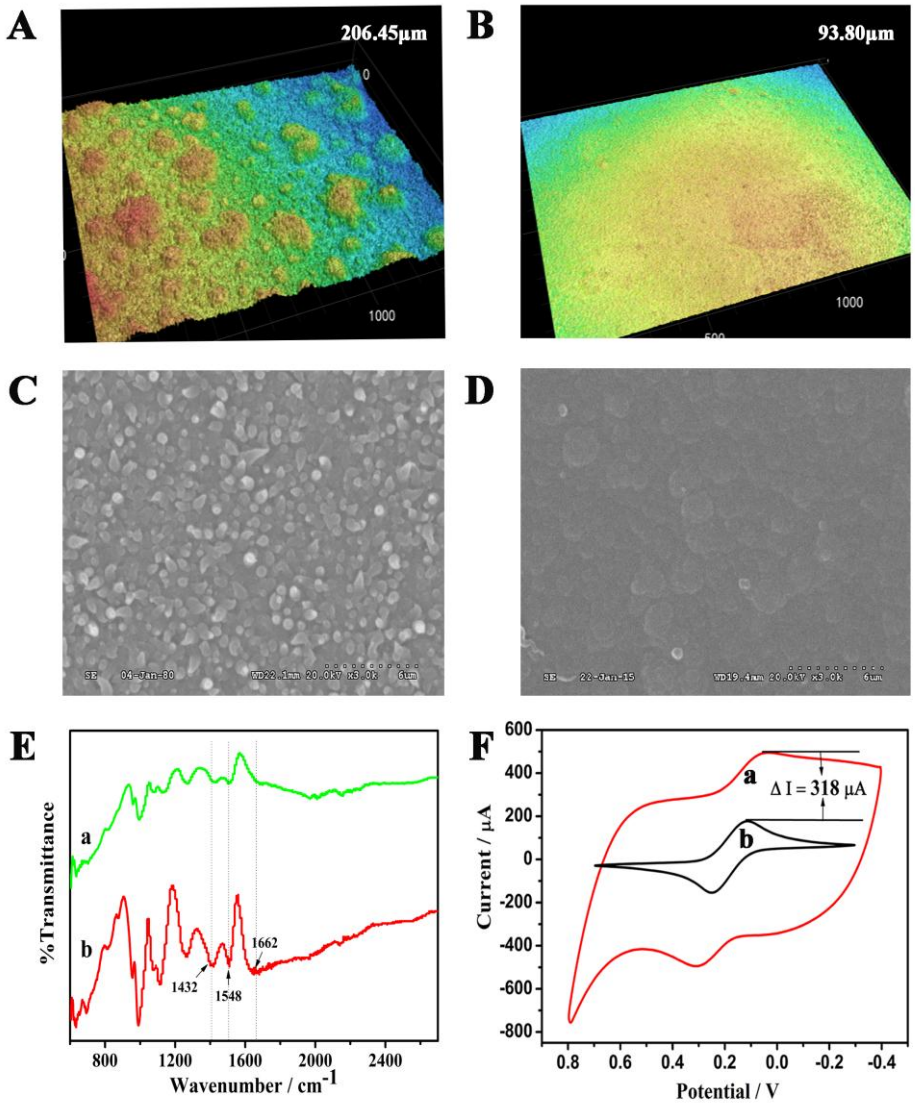

Fig. 1. 3D laser scanning images of (A) PPy and (B) PPy/streptavidin. SEM images of (C) PPy and (D) PPy/streptavidin. (E) FT-IR spectrum and (F) the CVs of PPy (curve a) and PPy/streptavidin (curve b) were performed in a 5 mM $[Fe(CN)_6]^{3-/4-}$ solution containing 0.1 M KCl.

3.2. Characterization of the Au-PAMAM-CP bionanocomposite probe

Au-PAMAM and Au-PAMAM-CP were characterized by TEM, HRTEM, FT-IR spectroscopy and UV-vis spectroscopy. Fig. 2 shows the morphology of Au-PAMAM and Au-PAMAM-CP. The TEM and HRTEM results inferred that the Au spherical nanoparticles were of a uniform diameter of 1 nm and were surrounded by PAMAM

dendrimers. Each Au nanoparticle was bound to more than one PAMAM dendrimer molecule through amino-Au affinity and was greatly separated from each other and homogeneously spread out on the PAMAM. Interestingly, as shown in Fig. 2B and C, after the binding of CP, a flower-like Au-PAMAM-CP bionanocomposite probe was formed. Moreover, we observed that the Au-PAMAM-CP was well-organized and well-dispersed with a diameter of approximately 40 nm.

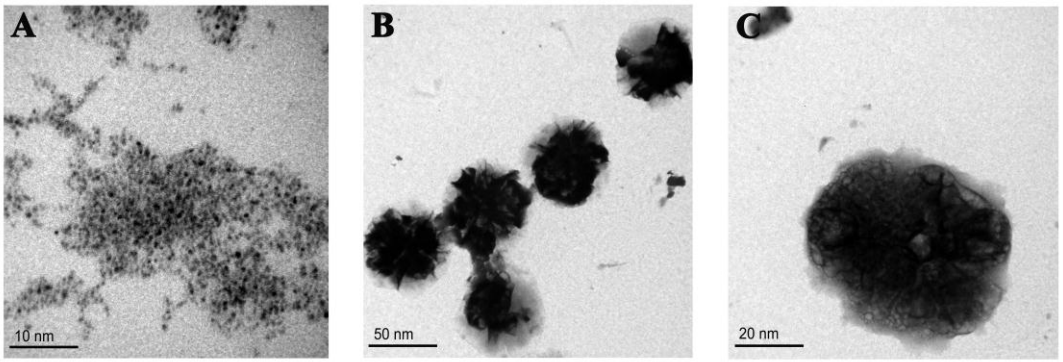

Fig. 2. TEM images of the Au-PAMAM (A), Au-PAMAM-CP bionanocomposite probe (B), and HRTEM of Au-PAMAM-CP bionanocomposite probe (C).

Fig. 3 shows evidence for the formation of Au-PAMAM, as investigated by FT-IR spectroscopy and UV-vis spectroscopy. As shown in Fig. 3A, the peak at 1449 cm^{-1} suggests a strong perturbation of the amide by the presence of nanoparticles. Additionally, a new absorption peak for PAMAM-Au appears at approximately 1665 cm^{-1}; this peak also confirms the formation of Au-PAMAM (Crespilho et al. 2006). Fig. 3C shows the UV-vis spectra of PAMAM-$HAuCl_4$, PAMAM and Au-PAMAM. PAMAM (curve a) exhibited absorption peaks at approximately 280 nm (Su and Tzou 2012). In PAMAM-$HAuCl_4$ (curve b), before reduction, $AuCl_4^-$ shows a ligand-metal charge-transfer band at 220 nm and a shoulder at 290 nm (Giorgetti et al. 2007). After reduction with $NaHB_4$, the spectrum changes significantly: the 220-nm band of $AuCl_4^-$ vanished, and a higher absorption intensity at low energy, a peak at 528 nm, is also observed (curve c) due to the formation of AuNPs.

ACCEPTED MANUSCRIPT

UV-vis absorption spectrum analysis also provides more effective information on the successful formation of Au-PAMAM-CP. Fig. 3D shows the UV-vis absorption spectra of PAMAM, CP and Au-PAMAM-CP. The absorption spectrum of the PAMAM (curve a) exhibits a characteristic peak at 290 nm (An et al. 2012). The characteristic absorption peak at 260 nm (Huang et al. 2015) is observed for the CP (curve b). After the formation of Au-PAMAM-CP (curve c), the absorption spectrum was expected to show the characteristic absorption peaks of CP, PAMAM and AuNPs. However, the characteristic absorption peak appears at 270 nm, probably because it corresponds to the characteristic peak of PAMAM and CP. Moreover, the characteristic absorption peaks at 530 nm correspond to the characteristic peaks of AuNPs (Giorgetti et al. 2007), which indicates that CP was attached to Au-PAMAM successfully.

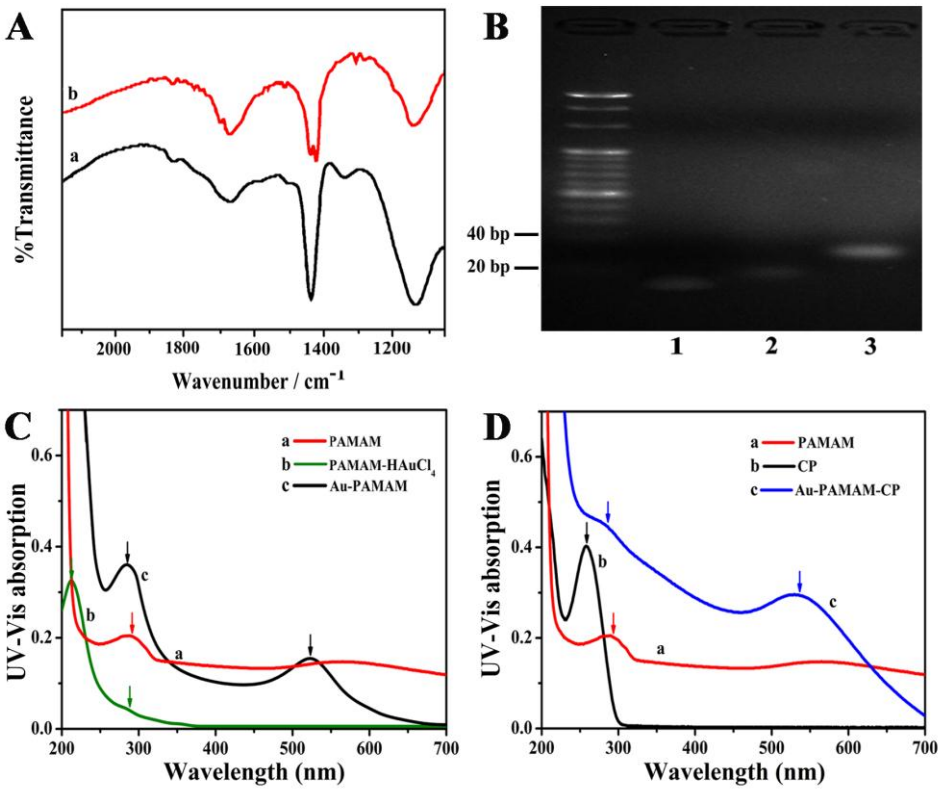

Fig. 3. FT-IR spectra for (A) (a) PAMAM and (b) Au-PAMAM. (B) Agarose gel electrophoresis of CP and target DNA conjugate. Lane 1: target DNA. Lane 2: CP. Lane 3: reaction mixture. UV-Vis spectroscopy of (C) (a) PAMAM, (b) PAMAM-

ACCEPTED MANUSCRIPT

$HAuCl_4$, (c) Au-PAMAM and (D) (a) PAMAM, (b) CP, (c) Au-PAMAM-CP.

3.3. Characterization of CP

The successful coupling of the target DNA and CP was investigated by agarose gel electrophoresis. From Fig. 3B, one can see that the low-molecular-weight target DNA, approximately 18 bp (lane 1), showed the highest mobility in lane 1 due to its low molecular weight, whereas, as expected, CP-target DNA conjugates showed the lowest mobility in lane 3. The result is similar to the results reported by Groves (Kroiss et al. 2014) and Fischer (Coyle et al. 2013) on the production of the CP-target DNA conjugates.

3.4. Electrochemical characteristics of the stepwise modified electrodes

CV and EIS were applied to characterize the modification steps of the DNA biosensor using $[Fe(CN)_6]^{3-/4-}$ as a redox probe, and were performed in a 5 mM $[Fe(CN)_6]^{3-/4-}$ solution containing 0.1 M KCl. The CV measurements were carried out within a scan rate of 50 mV s^{-1} and a voltage range of -0.3 V to 0.7 V. The EIS parameters employed included a 5 mV amplitude and frequency range of 1×10^{-3}-1×10^{-5} Hz at room temperature. Fig. 4A shows the superimposed CVs of $[Fe(CN)_6]^{3-/4-}$ recorded for a bare gold electrode (a), PPy/streptavidin-modified gold electrode (b), after incubation with BSA solution (1 wt%) (c), and after immobilization of the Au-PAMAM-CP-target DNA (d). As shown below, a pair of typical reversible redox peaks of ferricyanide ions can be observed on the bare gold electrode (Fig. 4A, curve a). A sharp increase was found on the PPy/streptavidin-modified gold electrode (Fig. 4A, curve b), which demonstrated that the PPy/streptavidin that was produced had an enhanced electrochemical signal compared to bare gold electrode. After the PPy/streptavidin-modified electrode was immersed into a BSA solution (Fig. 4A, curve c) and further incubated with a Au-PAMAM-CP-target DNA solution (Fig. 4A, curve d), the peak current increased, which was attributed to the hybridization of CP

Accepted manuscript

and target DNA. As shown in Fig. 4B, the EIS results were in agreement with the conclusions obtained from CVs, and the equivalent circuit (top right corner of Fig. 4B) was used to fit the impedance spectra. This circuit includes C_{dl}, which is a constant phase element CPE related to the double layer capacitance; R_S (electrolyte solution); Z_W (Warburg impedance), which caused the diffusion of the redox probe ions to the electrode interface from the bulk of the electrolyte; and R_{et} (resistance of the electron transfer). The values obtained after fitting the resistance spectra are recorded in Table 1. The above results indicated the successful fabrication of the DNA biosensor.

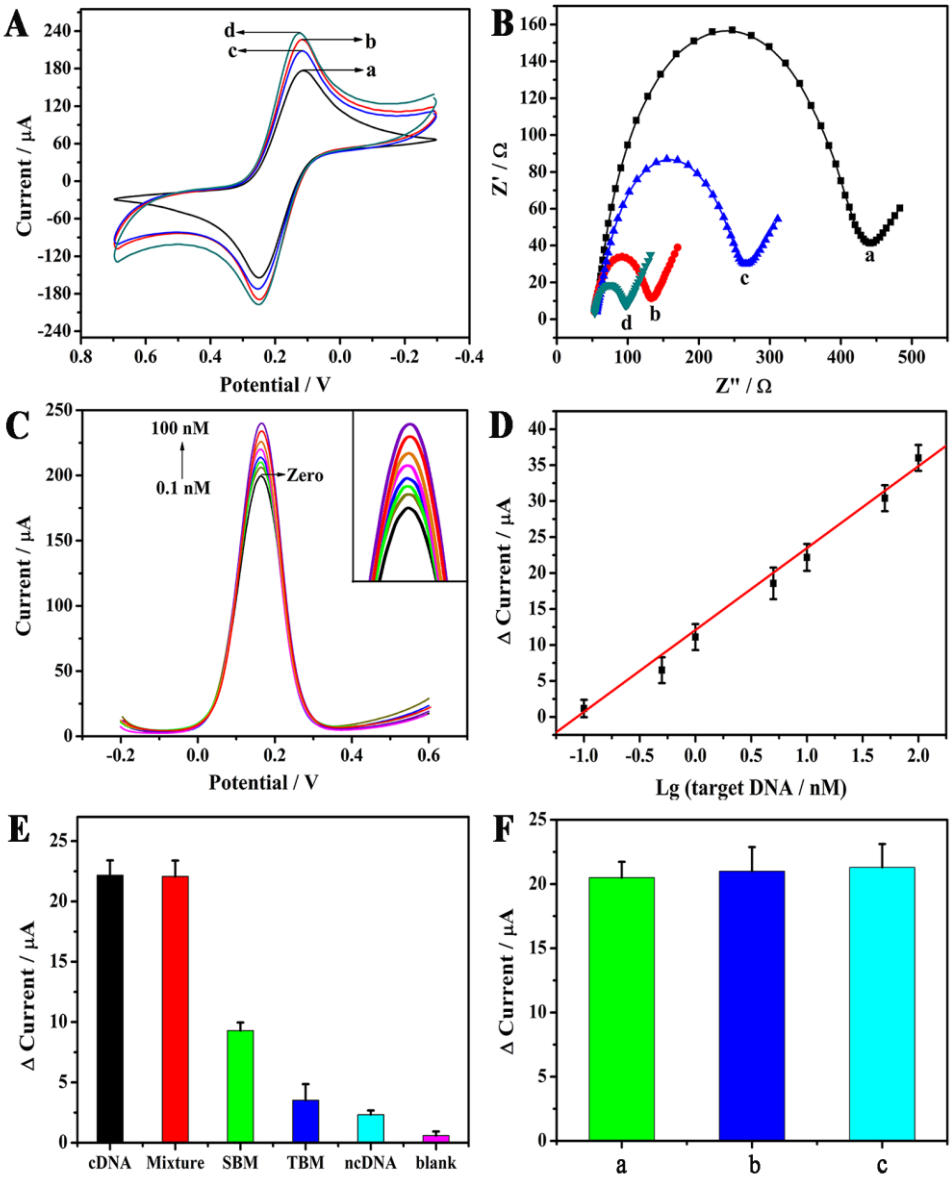

Fig. 4. CV, EIS and DPV were performed in a 5 mM $[Fe(CN)_6]^{3-/4-}$ solution

ACCEPTED MANUSCRIPT

containing 0.1 M KCl: (A) CVs (scan rate: 50 mV s^{-1}, voltage range: -0.3 V to 0.7 V) and (B) the EIS (amplitude: 5 mV, frequency range: 1×10^{-3}-1×10^{-5} Hz) of (a) bare gold electrode, (b) PPy/streptavidin/Au, (c) BSA/PPy/streptavidin/Au, and (d) Au-PAMAM-CP-target DNA/BSA/PPy/streptavidin/Au. (C) DPV response of the DNA biosensor assays with an increasing cDNA concentration of 0.1, 1, 10, 50 and 100 nM and (D) the resulting calibration plot. (E) The specificity of the biosensor was investigated with four types of 10 nM ssDNA: Mixture, single-base mismatched DNA (SBM), three-base mismatched DNA (TBM), non-complementary DNA (ncDNA) and blank control. Error bars are standard deviations across three repetitive experiments. (F) Investigation of the matrix effect: The comparison of the DPV signals of 10 nM cDNA in hybridization buffer (a), and in 5% serum (b) or 10% serum (c).

Table 1

Simulation parameters of the equivalent circuit components from Fig. 4B

Electrode	R_s (MΩ cm^2)	R_{et} (MΩ cm^2)	C_{dl} (μF cm^2)	n	$10^3 Z_w$ (MΩ cm^2)
GE	7.04	44.64	19.82	0.91	1.52
PPy/avidin	6.59	9.29	13.95	0.92	0.40
blocking with 1% BSA	7.17	24.63	31.69	0.89	1.22
Au-PAMAM-CP-target DNA	6.67	4.99	14.72	0.94	0.30

3.5. Optimization of the experimental conditions

The optimum conditions (the deposition time, hybridization temperature, hybridization time, and capture time) were determined, as shown in Fig. S1. A de tailed description can be found in the Supplementary information (S13)

3.6. Analytical performance of the electrochemical DNA biosensing approach

The electrochemical responses of $[Fe(CN)_6]^{3-/4-}$ toward different concentrations

Accepted manuscript

ACCEPTED MANUSCRIPT

of target DNA were measured by DPV under the optimal conditions. The lowest curve in Fig. 4C represents the baseline, and the peak current was linear to the DNA concentrations in the range of 0.1 to 100 nM (inset of Fig. 4C). As the target DNA concentration increased, more stem-loops of Au-PAMAM-CP opened, which led to more Au-PAMAM emerged on the electrode surface. As a result, the peak current increased. Furthermore, the data were analysed using statistical correlation calculations, and a linear relationship was observed between the peak current and target DNA concentrations in the range of 0.1 nM to 100 nM. The linear equation was I = 11.599*log C+11.198, with a correlation coefficient of 0.996. The detection limit was determined to be 0.033 nM based on the 3 s κ^{-1} rule (where s is the relative standard deviation of a blank solution and κ is the slope of the corresponding calibration curve). The proposed biosensor exhibited a satisfactory detection limit and linear range.

3.7. Specificity, repeatability, and stability of the DNA biosensing approach

For the DNA biosensor, the specificity affected the detection performance. As shown in Fig. 4E, we performed a comparison study between mismatched targets (SBM, TBM, ncDNA), a perfect complementary target (cDNA) and a blank control. Repeatability is another important criterion for DNA biosensors: five modified electrodes were used to detect cDNA (10 nM), and the relative standard deviation (RSD) was 3.1%, suggesting that the reproducibility of the DNA biosensor is acceptable. Furthermore, the DNA biosensor remained bioactive after two weeks of storage at 4°C, and the current response showed no significant changes. The result demonstrates that the developed electrochemical DNA biosensor has satisfactory stability.

3.8. Application in the analysis of serum samples

Accepted manuscript

ACCEPTED MANUSCRIPT

To exclude the potential interfering species, the validity of the proposed signal amplification strategy to real clinical samples was investigated. We challenged our sensing strategy with the presence of target DNA in a complex sample matrix: 5% and 10% human serum. Target DNA (10 nM) was spiked into the human serum and was assayed using the developed DNA biosensor. As shown in Fig. 4F, there is no obvious current change, which demonstrated the capacity of this assay for the analysis of real samples in which the influence of the matrix could be neglected. To examine the applicability of the present DNA biosensor to biological samples, the biosensor was used to test the recoveries of three concentrations of the target DNA. In this study, the real samples were prepared by a standard addition method. Each concentration was measured three times using five different electrodes with DPV analysis. It can be observed from Table S1 that the relative standard deviation was in the range of 3.22% to 4.45% and the recovery was in the range of 103% to 105%.

4. Conclusions

In summary, this is the first report of the use of PPy/streptavidin as a modified matrix material and a new Au-PAMAM-CP nanocomposite probe for a DNA hybridization detection method in a electrochemical biosensor. Au-PAMAM-CP-Target DNA signal is different in the $[Fe(CN)_6]^{3-/4-}$ enabled us to propose a novel non-immobilizing DNA sensing strategy that does not require the analytes to be labelled. The CP is applicable to the sensitive discrimination of complementary DNA from non-complementary sequences. This assay protocol is simple, convenient and cost-effective. Moreover, it can be successfully applied to quantify sequence-specific DNA in serum samples, particularly for the fast quantitative detection of the *vangl1* gene for the early diagnosis of NTDs. We propose that this assay might be a promising approach to perform DNA-based diagnostics.

Accepted manuscript

Acknowledgments

ACCEPTED MANUSCRIPT

This work was supported by grants from the National Natural Science Foundation of China (No. 31271246, No. 81370403)

References

An, Y., Jiang, X., Bi, W., Chen, H., Jin, L., Zhang, S., Wang, C., Zhang, W., 2012. Biosens. Bioelectron. 32, 224-230.

Bradbury, I.R., Hamilton, L.C., Dempson, B., Robertson, M.J., Bourret, V., Bernatchez, L., Verspoor, E., 2015. Mol. Ecol. 24, 5130-5144.

Byler, D.M., Susi, H., 1986. Biopolymers. 25, 469-487.

Cai, C., Shi, O., Wang, B., Chang, B., Yang, R., Wang, Y., Wang, F., Shen, C., 2014. Neuropediatrics. 45, 234-239.

Chang, K., Deng, S., Chen, M., 2015. Biosens. Bioelectron. 66, 297-307.

Chen, J., Zhou, S., 2015. Biosens. Bioelectron. 77, 277-283.

Cosnier, S., 1999. Biosens. Bioelectron. 14, 443-456.

Coyle, M.P., Xu, Q., Chiang, S., Francis, M.B., Groves, J.T., 2013. J. Am. Chem. Soc. 135, 5012-5016.

Crespilho, F.N., Zucolotto, V., Brett, C.M., Oliveira, O.N., Nart, F.C., 2006. J. Phys. Chem. B. 110, 17478-17483.

Fu, X., Cheng, Z., Yu, J., Choo, P., Chen, L., Choo, J., 2016. Biosens. Bioelectron. 78, 530-537.

Fujii, K., Matsubara, Y., Akanuma, J., Takahashi, K., Kure, S., Suzuki, Y., Imaizumi, M., Iinuma, K., Sakatsume, O., Rinaldo, P., Narisawa, K., 2000. Hum. Mutat. 15, 189-196.

Ghanbari, K., Hajheidari, N., 2015. Anal. Biochem. 473, 53-62.

Giorgetti, E., Giusti, A., Giammanco, F., Laza, S., Del Rosso, T., Dellepiane, G., 2007. Appl. Surf. Sci. 254, 1140-1144.

Huang, X., Huang, X., Zhang, A., Zhuo, B., Lu, F., Chen, Y., Gao, W., 2015. Biosens. Bioelectron. 70, 441-446.

Jeong, B., Akter, R., Han, O.H., Rhee, C.K., Rahman, M.A., 2013. Anal. Chem. 85, 1784-1791.

Jo, H., Her, J., Ban, C., 2015. Biosens. Bioelectron. 71, 129-136.

Kavosi, B., Salimi, A., Hallaj, R., Amani, K., 2014. Biosens. Bioelectron. 52, 20-28.

Kjällman, T.H., Peng, H., Soeller, C., Travas-Sejdic, J., 2008. Anal. Chem. 80, 9460-9466.

Li, Y., Fang, L., Cheng, P., Deng, J., Jiang, L., Huang, H., Zheng, J., 2013. Biosens. Bioelectron. 49, 485-491.

Kroiss, M., Brünger, K.M., Wiesner, J., Grimmler, M., Sickmann, A., Fischer, U., 2014. Fly 3, 223-231.

Li, Y., Wen, Y., Wang, L., Liang, W., Xu, L., Ren, S., Zou, Z., Zuo, X., Fan, C., Huang, Q., Liu, G., Jia, N., 2015. Biosens. Bioelectron. 67, 364-369.

Liang, L., Shen, J.W., Zhang, Z., Wang, Q., 2015. Biosens. Bioelectron.

Liu, G., Lao, R., Xu, L., Xu, Q., Li, L., Zhang, M., Song, S., Fan, C., 2013. Biosens. Bioelectron. 42, 516-521.

Livnah, O., Bayer, E.A., Wilchek, M., Sussman, J.L., 1993. P. Natl. Acad. Sci. USA. 90, 5076-5080.

Maekawa, K., Nakamura, R., Kaniwa, N., Mizusawa, S., Kitamoto, A., Kitamoto, T., Ukaji, M.,

Accepted manuscript

ACCEPTED MANUSCRIPT

Matsuzawa, Y., Sugiyama, E., Uchida, Y., Kurose, K., Ueta, M., Sotozono, C., Ikeda, H., Yagami, A., Matsukura, S., Kinoshita, S., Muramatsu, M., Ikezawa, Z., Sekine, A., Furuya, H., Takahashi, Y., Matsunaga, K., Aihara, M., Saito, Y., 2015. Pharmacogenomics. 16, 1689-1699.

Meyer, S., Trost, N., Frey, B.M., Gassner, C., 2015. Methods in molecular biology. 1310, 51-70.

Mogi, T., Hatakeyama, K., Taguchi, T., Wake, H., Tanaami, T., Hosokawa, M., Tanaka, T., Matsunaga, T., 2011. Biosens. Bioelectron. 26, 1942-1946.

Russom, A., Haasl, S., Brookes, A.J., Andersson, H., Stemme, G., 2006. Anal. Chem. 78, 2220-2225.

Mohamed, R., Desmond, P., Suh, D.J., Amarapurkar, D., Gane, E., Guangbi, Y., Hou, J.L., Jafri, W., Lai, C.L., Lee, C.H., Lee, S.D., Lim, S.G., Guan, R., Phiet, P.H., Piratvisuth, T., Sollano, J., Wu, J.C., 2004. J. Gastroenterol. Hepatol. 19, 958-969.

Ruiyi, L., Ling, L., Hongxia, B., Zaijun, L., 2015. Biosens. Bioelectron. 79, 457-466.

Shen, W.J., Zhuo, Y., Chai, Y.Q., Yang, Z.H., Han, J., Yuan, R., 2015. Acs. Appl. Mater. Inter. 7, 4127-4134.

Shin, Y., Soo, R.A., Yoon, J., Perera, A.P., Yoon, Y.J., Park, M.K., 2015. Biosens. Bioelectron. 68, 107-114.

Stepanov, V.A., Trifonova, E.A., 2013. Mol. Biol. 47, 852-862.

Su, P. G., Tzou, W. H., 2012. Sensor. Actuat. A-Phys. 179, 44-49.

Syvänen, A.C., 2001. Nat. Rev. Genet. 2, 930-942.

Tomalia, D.A., Frechet, J.M., 2002. Introduction to the dendritic state.1-44.

Wang, S., Wong, D., Forrest, K., Allen, A., Chao, S., Huang, B.E., Maccaferri, M., Salvi, S., Milner, S.G., Cattivelli, L., Mastrangelo, A.M., Whan, A., Stephen, S., Barker, G., Wieseke, R., Plieske, J., International Wheat Genome Sequencing, C., Lillemo, M., Mather, D., Appels, R., Dolferus, R., Brown-Guedira, G., Korol, A., Akhunova, A.R., Feuillet, C., Salse, J., Morgante, M., Pozniak, C., Luo, M.C., Dvorak, J., Morell, M., Dubcovsky, J., Ganal, M., Tuberosa, R., Lawley, C., Mikoulitch, I., Cavanagh, C., Edwards, K.J., Hayden, M., Akhunov, E., 2014. Plant. Biotechnol. J. 12, 787-796.

Wang, X., Hou, T., Dong, S., Liu, X., Li, F., 2016. Biosens. Bioelectron. 77, 644-649.

Xiao, Y., Li, C.M., Liu, Y., 2007. Biosens. Bioelectron. 22, 3161-3166.

Yao, G.H., Liang, R.P., Huang, C.F., Wang, Y., Qiu, J.D., 2013. Anal. Chem. 85, 11944-11951.

Zhang, Q., Wang, N., Zhao, L., Xu, T., Cheng, Y., 2013. ACS. Appl. Mater. Inter. 5, 1907-1912.

Zhuo, Y., Yuan, R., Chai, Y. Q., Hong, C. L., 2010. Analyst. 135, 2036.

Zong, J., Yang, X., Trinchi, A., Hardin, S., Cole, I., Zhu, Y., Li, C., Muster, T., Wei, G., 2013. Nanoscale. 5, 11200-11206.

Accepted manuscript

Highlights:

1. A novel DNA biosensor to detect the rs4839469 locus of VANGL1 gene for dysontogenesis prediction has been developed for the first time.

ACCEPTED MANUSCRIPT

2. PPy/streptavidin, which as modified matrix material, and Au-PAMAM-CP nanocomposite probe, a novel probe, were used for the rs4839469 locus of VANGL1 gene detection.

3. Wide linear range, good specificity and high sensitivity of the sensor have been achieved.

Accepted manuscript